OXFORD

Cerebral Cortex, January 2021;31: 32–47

doi: 10.1093/cercor/bhaa201
Advance Access Publication Date: 22 August 2020
Original Article

ORIGINAL ARTICLE

Layer-Specific Inhibitory Microcircuits of Layer 6 Interneurons in Rat Prefrontal Cortex

Chao Ding[1], Vishalini Emmenegger[1,4], Kim Schaffrath[1,5] and Dirk Feldmeyer[1,2,3]

[1]Institute of Neuroscience and Medicine, INM-10 Function of Cortical Microcircuits Group, Research Centre Jülich, 52425 Jülich, Germany, [2]Department of Psychiatry, Psychotherapy and Psychosomatics, Medical School, RWTH Aachen University Hospital, 52074 Aachen, Germany, [3]JARA-Translational Brain Medicine, 52074 Aachen, Germany, [4]Current address: Department of Biosystems Science and Engineering, ETH Zürich, Basel, Switzerland and [5]Current address: Department of Ophthalmology, RWTH Aachen University Hospital, Medical School, 52074 Aachen, Germany

Address correspondence to Prof. Dr Dirk Feldmeyer, Institute of Neuroscience and Medicine, INM-10 Function of Cortical Microcircuits Group, Research Centre Jülich, 52425 Jülich, Germany. Email: d.feldmeyer@fz-juelich.de
Chao Ding and Vishalini Emmenegger have contributed equally to this work.

Abstract

GABAergic interneurons in different cortical areas play important roles in diverse higher-order cognitive functions. The heterogeneity of interneurons is well characterized in different sensory cortices, in particular in primary somatosensory and visual cortex. However, the structural and functional properties of the medial prefrontal cortex (mPFC) interneurons have received less attention. In this study, a cluster analysis based on axonal projection patterns revealed four distinct clusters of L6 interneurons in rat mPFC: Cluster 1 interneurons showed axonal projections similar to Martinotti-like cells extending to layer 1, cluster 2 displayed translaminar projections mostly to layer 5, and cluster 3 interneuron axons were confined to the layer 6, whereas those of cluster 4 interneurons extend also into the white matter. Correlations were found between neuron location and axonal distribution in all clusters. Moreover, all cluster 1 L6 interneurons showed a monotonically adapting firing pattern with an initial high-frequency burst. All cluster 2 interneurons were fast-spiking, while neurons in cluster 3 and 4 showed heterogeneous firing patterns. Our data suggest that L6 interneurons that have distinct morphological and physiological characteristics are likely to innervate different targets in mPFC and thus play differential roles in the L6 microcircuitry and in mPFC-associated functions.

Key words: axonal projection, interneurons, layer 6, medial prefrontal cortex

Introduction

Seminal research in rats, monkeys, and humans has revealed that the prefrontal cortex (PFC) plays an essential role in emotional regulation and executive function including cognitive processes such as memory, attention, and decision-making (Fuster 2001; Miller and Cohen 2001; Euston et al. 2012; Fuster 2015; Hiser and Koenigs 2018). While the rodent PFC is undoubtedly less complex than its human counterpart, it nevertheless encompasses similar executive functions. The rodent PFC acts like a nodal station of cortical networks by receiving multimodal cortico-cortical projections, such as from motor, somatosensory, gustatory, limbic, and auditory cortices (Brown and Bowman 2002; Uylings et al. 2003; Leonard 2016). The medial prefrontal cortex (mPFC), which includes the anterior cingulate cortex, prelimbic cortex, and infralimbic cortex, consists of 80–90% glutamatergic pyramidal cells and 10–20% GABAergic interneurons

(Riga et al. 2014). GABAergic interneurons in sensory cortices have been classified with respect to their morphological, functional, and molecular properties (for reviews see Markram et al. 2004; Ascoli et al. 2008; DeFelipe et al. 2013; Kepecs and Fishell 2014; Lein et al. 2017; Zeng and Sanes 2017; Yuste et al. 2019). By analogy, mPFC interneurons can be identified based on similar parameters.

GABAergic interneurons play a significant role in orchestrating network activity by regulating the concerted activity of pyramidal cells (for a review see Tremblay et al. 2016). Pyramidal cells of virtually all cortical layers are endowed with different active properties, including Na^+ action potentials initiated at the axon initial segment, Ca^{2+} plateau spikes initiated at the initial bifurcation of the apical dendritic tuft, local Na^+ spikelets generated in the dendrites and NMDA receptor-mediated spikes in the distal basal and apical dendrites (Larkum et al. 1999; Larkum et al. 2007; Ledergerber and Larkum 2010; for a review see Larkum 2013). The interaction between these regions of excitability has been suggested to serve the detection of coincident synaptic inputs, synaptic gain control, and the coordination and association of activity in different cortical areas. It has been proposed to be involved in learning processes and consciousness. Different types of interneurons innervate different subcellular compartments of pyramidal cells, thereby providing a spatiotemporal control of the integration and gain of incoming synaptic activity (e.g., at the basal dendrites and apical tuft; Palmer et al. 2012; Lee et al. 2015). Alterations of specific inhibitory circuits can have dramatic consequences for intracortical signal processing resulting in neuropsychiatric conditions, among them schizophrenia, anxiety, or depression (Benes and Berretta 2001; Volk and Lewis 2005; Beneyto et al. 2011; Mohler 2012; Zorrilla de San Martin et al. 2020).

In order to understand neuronal circuit dynamics at the local level, it is crucial to investigate the different interneuron types and their connectivity pattern in different cortical layers. In sensory cortices, the heterogeneity of interneurons is well characterized (for reviews see e.g., Ascoli et al. 2008; Feldmeyer et al. 2018; Yuste et al. 2019). However, only few studies on the diversity of interneurons in the mPFC are currently available most of which are qualitative and focused on superficial cortical layers (Gabbott and Bacon 1996, 1997; Gabbott et al. 1997; Krimer and Goldman-Rakic 2001; Krimer et al. 2005; Zaitsev et al. 2009; Rotaru et al. 2015). This is surprising as layer 6 (L6) of mPFC emerges as a key player in attention control (Wimmer et al. 2015). L6 excitatory neurons in sensory cortices project extensively to many other cortical areas such as other sensory cortices, the motor cortex, and the PFC, as well as subcortical regions including thalamic nuclei and to local circuit interneurons in cerebral cortex (Zhang and Deschenes 1997, 1998; Guillery and Sherman 2002; Thomson et al. 2002; West et al. 2006; Zikopoulos and Barbas 2006; Kumar and Ohana 2008; Thomson 2010; Pichon et al. 2012; Arzt et al. 2018). In PFC, deep layer excitatory neurons project to both the mediodorsal and the ventromedial nucleus of the thalamus, which in turn projects predominantly to layer 2/3 (Krettek and Price 1977; Gabbott et al. 2005; Collins et al. 2018). These PFC inputs to thalamus play a key role in sustaining persistent activity during behavior (Schmitt et al. 2017) and are likely to be under the control of local inhibitory synaptic inputs. So far, little is known about the interneuron complement of this associative cortical area and the axonal projection motifs and connectivity profiles of the deep layer PFC interneurons. To understand the complexity of the L6 microcircuitry, it is pivotal to identify not only the excitatory but also the inhibitory neuron complement of this layer. Quantitative measures of axonal projections are considered to be of high functional significance because they are one of the parameters defining neuronal innervation domains, thereby making a reliable prediction of synaptic connectivity possible (Lubke et al. 2003; Feldmeyer et al. 2018). Therefore, we used axonal projections with reference to layer borders and soma position as primary classifiers and employed classification methods such as unsupervised cluster analysis to identify different interneuron types in L6 of rat mPFC. We found that L6 interneurons display layer-specific axonal projections, for instance local L6 projecting interneurons and translaminar projecting interneurons, which were further subdivided into locally projecting interneurons, L6/white-matter (WM)-projecting interneurons, L5-projecting interneurons, and L1/2/3-projecting interneurons. For some mPFC L6 interneuron types a correlation between electrophysiological properties and axonal projection pattern was found.

Materials and Methods

Slice Preparation

All experimental procedures were carried out in accordance with the guidelines of the Federation of European Laboratory Animal Science Association (FELASA), the EU Directive 2010/63/EU, and the German animal welfare act and were approved by the Northrhine-Westphalian Landesamt für Natur-, und Verbraucherschutz (LANUV).

In this study, Wistar rats (Charles River, either sex) aged 17–21 postnatal days (P17–21) were used. The experimental procedures used here have been described previously (van Aerde and Feldmeyer 2015). Briefly, rats were deeply anesthetized with isoflurane and decapitated. The brain was quickly removed and placed in an ice-cold artificial cerebrospinal fluid (ACSF) containing 125 mM NaCl, 2.5 mM KCl, 1.25 mM NaH_2PO_4, 4 mM $MgCl_2$, 1 mM $CaCl_2$, 25 mM $NaHCO_3$, 25 mM glucose, 3 mM myo-inositol, 2 mM Na-pyruvate, and 0.4 mM ascorbic acid; the osmolarity of the solution was ~310 mOsm. The concentration of Ca^{2+} was lowered to reduce potential excitotoxic synaptic transmission during slicing. In order to maintain adequate oxygenation and a physiological pH level, the solution was constantly bubbled with carbogen gas (95% O_2 and 5% CO_2). 350 µm thick coronal slices of the prelimbic mPFC were cut using a vibrating microslicer at a low speed and high vibration frequencies. The slices were then transferred to an incubation chamber for a recovery period of ~1 h at room temperature.

During whole-cell patch-clamp recordings, slices were continuously perfused (perfusion speed ~5 mL/min) with an artificial ACSF containing: 125 mM NaCl, 2.5 mM KCl, 1.25 mM NaH_2PO_4, 1 mM $MgCl_2$, 2 mM $CaCl_2$, 25 mM $NaHCO_3$, and 25 mM glucose, bubbled with carbogen gas and maintained at ~31 °C. Patch pipettes were pulled from thick-wall borosilicate glass capillaries and filled with an internal solution containing 135 mM K-gluconate, 4 mM KCl, 10 mM HEPES, 10 mM phosphocreatine, 4 mM Mg-ATP, and 0.3 mM GTP (pH 7.4 with KOH, osmolarity ~300 mOsm). In order to obtain permanent stainings of the patched neurons for the morphological analysis, biocytin (0.5%) was added to the internal solution.

Neurons were visualized using infrared differential interference contrast microscopy. The layers were distinguished based on the cell density and cell soma size in agreement

with earlier studies on the PFC (Van Eden and Uylings 1985; Uylings and van Eden 1990; Gabbott et al. 1997; Gabbott et al. 2005; van Aerde and Feldmeyer 2015). Overall, the PFC can be divided into three sections—the upper third comprises L1–L3, the middle third includes L5 and the lower third constitutes L6 (Supplementary Fig. 1A). Unlike other cortical regions, L1 in PFC is distinctly wide. L2 is the thinnest layer of the PFC, and visible as a thin dark band between L1 and L3. Despite the lack of a granular layer, L3 and L5 is demarcated by a band of thalamocortical axon collaterals in deep L3 (Uylings and van Eden 1990; Uylings et al. 2003; Kubota et al. 2007; Hirai et al. 2012).

Electrophysiology

Whole-cell patch clamp recordings were made using an EPC10 amplifier (HEKA, Lambrecht, Germany). Signals were sampled at 10 kHz, filtered at 2.9 kHz using Patchmaster software (HEKA), and later analyzed off-line using Igor Pro software (Wavemetrics, USA). The recordings were performed using patch pipettes of resistance between 5 and 7 MΩ. After establishing the whole-cell configuration, the resting membrane potential was measured immediately after breakthrough. Bridge balance and capacitance neutralization were adjusted. Whole-cell series resistance was monitored throughout the experiment and was compensated by 80%. Recordings with a series resistance exceeding 50 MΩ were excluded from the data analysis. Membrane potentials were not corrected for the junction potential. Passive and active action potential properties were assessed by eliciting a series of initial hyperpolarizing, followed by depolarizing current pulses under current clamp configuration for 1 s. We used the intrinsic firing properties recorded in the current clamp mode to differentiate interneurons from pyramidal cells (Supplementary Fig. 1B), and morphological reconstructions for a post hoc confirmation (Supplementary Fig. 1C,D).

Histological Procedures

After the electrophysiological recordings, slices containing biocytin-filled neurons were fixed for at least 24 h at 4 °C in 100 mM phosphate buffer solution (PBS, pH 7.4) containing 4% paraformaldehyde (PFA). After rinsing slices several times in PBS, they were treated with 1% H_2O_2 in PBS for about 20 min, in order to reduce any endogenous peroxidase activity. Following this, slices were rinsed repeatedly using 100 mM PBS, then incubated in 1% avidin-biotinylated horseradish peroxidase (Vector ABC staining kit, Vector Lab. Inc.) containing 0.1% Triton X-100 for 1 h at room temperature. This was followed by a chromogenic reaction that resulted in a dark precipitate by adding 0.5 mg/ml 3,3-diaminobenzidine (DAB; Sigma-Aldrich, USA) until distinct axonal and dendritic branches of the biocytin-filled neurons were clearly visible. The slices were rinsed again with 100 mM PBS, followed by slow dehydration in increasing ethanol concentrations and finally in xylene for 2–4 h (Marx et al. 2012). Slices were then mounted on gelatinized slides and embedded using Eukitt medium (Otto Kindler GmbH).

Immunohistochemical Staining

For the identification of molecular markers expressed by GABAergic interneurons, 150 µm thin brain slices were prepared using a vibratome. Brain slices were immediately fixed with 4% PFA in 100 mM PBS for ~4 h at 4 °C. The slices were then permeabilized in 0.5% Triton X-100 in 100 mM PBS with 1% milk powder for 1 h at room temperature. Primary and secondary antibodies for parvalbumin (PV), somatostatin (SOM), and the transcription factor Prox1 were diluted in a permeabilization solution containing 0.5% Triton X-100 and 100 mM PBS. Subsequently, slices were incubated overnight at 4 °C in a solution containing the respective primary antibody and then rinsed thoroughly with 100 mM PBS. Slices were then treated with the secondary antibodies for 2–3 h at room temperature in the dark (see complete list of antibodies in Supplementary Table 1). Controls were also performed in the absence of primary and secondary antibodies. After rinsing several times in 100 mM PBS, slices were embedded in Moviol and visualized by transmitted light fluorescence microscopy using an upright microscope equipped with fluorescence optics. The fluorescence images were taken using the Olympus CellSens platform.

In a subset of experiments, we tried to identify the expression of molecular markers in single L6 interneurons in brain slices to investigate a possible correlation with the immunohistochemical, morphological and electrophysiological properties. To this end, Alexa Fluor 594 biocytin salt (1:500, Invitrogen, Darmstadt, Germany) was added to the internal solution (composition as described above) to identify the patched neurons in the post hoc antibody labelling methods. After recording, slices were fixed in 4% PFA in 100 mM PBS for 2–4 h at 4 °C and antibody labelling was performed as described above. The location of the stained neuron in the slice was visualized by the conjugated Alexa dye, so that the expression of a specific molecular marker could be tested in identified individual neurons. After acquiring fluorescent images, slices were incubated in 100 mM PBS overnight and subsequently processed for morphological analyses (see above).

Morphological 3D Reconstructions

Morphological reconstructions of biocytin filled Layer 6 mPFC interneurons were made using Neurolucida software (MicroBrightField, Williston, VT, USA) on an upright microscope equipped with a motorized stage at a magnification of 100-fold using oil-immersion objective. Neurons were selected for reconstruction based on the quality of biocytin labelling when background staining was minimal. Embedding using Eukitt medium reduced fading of cytoarchitectonic features and enhanced contrast between layers (Marx et al. 2012) (Supplementary Fig. 1C). This allowed the reconstruction of different layer borders along with the neuronal reconstructions (Supplementary Fig. 1D). Furthermore, the position of soma and layers were confirmed by superimposing the differential interference contrast images taken during the recording. All reconstructions were aligned with respect to the pial surface. The tissue shrinkage was corrected for using correction factors of 1.1 in the *x*–*y* direction and 2.1 in the z direction (Marx et al. 2012).

Data Analysis

Membrane and Spike Properties

Custom-written macros for Igor Pro 6 (Wavemetrics) were used for the analysis of the recorded electrophysiological data.

The resting membrane potential (V_{rest}) of the neuron was measured directly after breakthrough into the whole-cell configuration with no current injection. To calculate the input resistance (R_{in}), the slope of the linear fit to the voltage step from −60 to −70 mV of the current–voltage relationship was used (Ziegler et al. 2010). The rheobase current was defined as the minimal current that elicited the first spike.

For the analysis of single spike characteristics such as threshold, amplitude, and half-width, a smaller step size increment (10 pA) for current injection was used to ensure that the action potential was elicited very close to its potential threshold. The spike threshold was defined as the point of maximal acceleration of the membrane potential using the second derivative (d_2V/dt^2), that is, the time point with the fastest voltage change. The spike amplitude was calculated as the difference in voltage from AP threshold to the peak during depolarization. The spike half-width was measured as the time difference between rising phase and decaying phase of the spike at half-maximum amplitude. Interspike interval (ISI) was measured as the average time taken between individual spikes at the current step that elicited close to 10 APs. The adaptation ratio was measured as the ratio of the tenth ISI and the second ISI. In addition, the standard deviation (SD) of the ISI was used to describe the variability of ISI.

Morphological Properties

It has been reported that because of axonal truncations in slice preparations, the number of synapses made by inhibitory basket cell axons is markedly reduced (~40%) (Stepanyants et al. 2009). Therefore, we decided to include not all reconstructions but only a subset of neurons with an axon length exceeding 7 mm (i.e., the mean axon length of reconstructed PFC L6 interneurons) in the data analysis. Because our analysis is based on axonal projection patterns, it was crucial to determine the degree of axonal truncations in our 350 µm thick slices. To this end, cut axonal and dendritic endings were identified during the process of reconstruction. The number of high and low endings, (i.e. those truncated at the top and bottom of the slice, respectively) was determined. The percentage of truncations was calculated as the ratio of all high and low endings to the total number of endings. This ratio gives an approximation of the degree of axonal and dendritic truncation. Only reconstructions for which less than 15% of the total endings were truncated were used.

3D reconstructed neurons were quantitatively analyzed using Neuroexplorer software (MicroBrightField, Williston, VT, USA), Morphological properties such as the distributions of axonal length in cortical layer 1–6, the white matter, and the axonal orientation were extracted from Neuroexplorer software. The ratio of the axonal length in the horizontal and vertical directions was determined from polar histograms (in which spatial geometry is transformed into length and direction) and used to estimate the predominant axonal orientation.

Unsupervised Hierarchical Cluster Analysis

Classification of interneuron subtypes was performed using unsupervised hierarchical cluster analysis employing Ward's method (Ward 1963). This method utilizes a minimum variance criterion to combine cells into clusters at each stage, which minimizes the total within-cluster variance. Euclidean distance was used to calculate the variance. A dendrogram was constructed to visualize the distance at which clusters are combined.

2D Axon Distribution Maps and Vertical Axon Distribution Profiles

2D and 1D axon distribution maps were made by using custom-written software in Matlab (courtesy of Drs G. Qi and H. Wang). 3D maps of axonal density were obtained using computerized 3D reconstructions. The soma center of each neuron in a single cluster was aligned and given the coordinates of X, Y, Z = (0, 0, 0). By using the segment point analysis in the Neuroexplorer, the relative coordinates of the beginning and endpoint of each segment in the axonal trace were acquired. The 3D density map for a cluster was constructed for each reconstructed neuron in this cluster and then averaged in Matlab. The averaged density maps were smoothed using the 3D smoothing function with a Gaussian kernel (s.d = 50 µm) and isosurfaces were calculated at the 80 percentile. 2D axon distribution maps were made by showing the 3D map in a 2D way with only x axis and y axis. 1D axon density profiles were calculated at a resolution of 50 µm by extracting value of y axis. The average curve of single group was made by aligning the soma position of individual profile.

Statistics

All data are represented as mean ± standard deviation. Because the distribution of measured parameters was not normal, the Kruskal–Wallis test was used for statistical comparisons among all clusters; for comparison between two independent groups, Wilcoxon–Mann–Whitney test was used. Correlation analysis was performed by calculating Pearson correlation coefficients.

Results

L6 interneurons in rat PFC were recorded using whole-cell patch-clamp with simultaneous biocytin filling. A widely used criterion to identify a neuron as an interneuron is the fact that its dendrites possess no or if at all very little dendritic spines. We calculated the average spine density per 10 µm dendrite in all our biocytin-labeled neurons identified in this study, which was found to be 0.29 ± 0.18 for all types of interneurons, a value significantly lower than that for pyramidal cells (Elston 2003; Arzt et al. 2018). This indicates that these neurons are GABAergic interneurons. In addition, firing patterns of excitatory and inhibitory neurons are very distinctive (Connors and Gutnick 1990) and are used in virtually all studies on GABAergic interneurons as a classification criterion. Finally, in a few instances we performed recordings from synaptically coupled neuron pairs and were able to show that these neurons are indeed GABAergic (Supplementary Fig. 1B). In a subset of experiments in which the expression of specific interneuron marker proteins was tested, the red fluorescent dye Alexa 594 was added together with biocytin to identify the location of the patched neurons prior to antibody labelling.

Morphological Classification of L6 Interneurons

All L6 interneurons with an axon length exceeding 7 mm were selected for further analysis, resulting in a total of 48 high-quality 3D morphological reconstructions. Quantitative morphological classification of L6 interneurons was performed based on their axonal projection patterns. Specifically, parameters used for cluster analysis were the distribution of the axonal

Table 1 Statistical analysis of the axonal properties of L6 inhibitory neurons in the four morphological clusters

Parameters	C1	C2	C3	C4	P value
Axonal distribution in L1–L3 (%)	37.2 ± 7.5	1.1 ± 2.3	0.2 ± 0.8	1.9 ± 3.6	5.9E-04
Axonal distribution in L5 (%)	41.2 ± 13.1	52.4 ± 18.0	8.0 ± 7.1	4.3 ± 5.9	1.62E-12
Axonal distribution in L6 (%)	20.8 ± 16.2	44.3 ± 18.2	88.3 ± 8.7	67.0 ± 16.7	1.16E-12
Axonal distribution in WM (%)	0.4 ± 0.7	2.2 ± 2.7	3.5 ± 3.3	26.8 ± 13.2	2.12E-07
Axonal distribution from Pia-Soma (%)	86.7 ± 8.6	79.2 ± 14.5	45.4 ± 20.7	32.7 ± 17.8	9.39E-09
Axonal distribution from Soma-WM (%)	13.3 ± 8.6	20.8 ± 14.5	54.6 ± 20.7	67.3 ± 17.8	9.39E-09
Relative soma position in L6	0.15 ± 0.09	0.21 ± 0.08	0.35 ± 0.13	0.63 ± 0.09	1.8E-09
Axon horizontal/vertical	0.73 ± 0.16	1.08 ± 0.22	1.20 ± 0.24	1.29 ± 0.43	0.006

All data are represented as mean ± standard deviation. The distribution of the axon in the different layers are given as percentage values. The Kruskal–Wallis test was used to test for the significant difference between clusters.

length in cortical layers 1–6 and the white matter (WM), the axon orientation, and the axonal distribution with respect to the soma position in layer 6 (from the pial surface to the soma and from the soma to the WM; see Materials and Methods). Based on these morphological parameters, four clusters were identified with distinct axonal projection patterns: L1/2/3-projecting interneurons, L5-projecting interneurons, locally projecting L6 interneurons and L6/WM-projecting interneurons (Fig. 1A, Supplementary Figs 2 and 3).

Morphological Cluster 1: L1/2/3-Projecting Interneurons

Of the 48 interneurons, five were L1/2/3-projecting interneurons constituting 10% of the population. All showed a largely vertical axonal projection pattern (axon horizontal/vertical: 0.73 ± 0.16, example in Fig. 1B, all reconstructions in Supplementary Fig. 2A). Compared with PFC L6 interneurons in clusters 2–4 (see below), a significantly larger fraction of the axonal collaterals of cluster 1 L6 interneurons resided in L1–L3 (37.2 ± 7.5%, $P = 5.9E-04$ between all clusters; Table 1). However, the axon plexus in L6 was significantly smaller (20.8 ± 16.2%, $P = 1.16E-12$ between all clusters; Table 1). All cluster 1 L6 interneurons had axon collaterals terminating in L1. Two of them showed horizontally projecting collaterals in L1, while the other three cluster 1 interneurons sent several collaterals to L5 and L3. The relative soma position of these PFC L6 interneurons in their home layer was calculated as the ratio between the distance from soma to the L5/L6 border and the vertical length of L6. L1/2/3-projecting interneurons had an average soma position value of 0.15 ± 0.09 (Fig. 2A), that is, they were located near the L5/L6 border; their axon collaterals projected mostly toward the pial surface (ratio of axonal distribution from pia to soma: 0.87 ± 0.09, Fig. 2). In addition, the number of axonal bouton in layer 1/2/3 was 18.9 ± 4.9/100 µm ($n = 5$), which was significantly higher than that in layer 6 (13.1 ± 2.0/100 µm) suggesting a higher probability of establishing synaptic contacts.

Morphological Cluster 2: L5-Projecting Interneurons

The second cluster, the L5-projecting interneurons, consisted of 15 interneurons and constituted 31% of the L6 interneuron population. Like L1/2/3-projecting interneurons, these interneurons were also located near the L5/6 border (relative soma position: 0.21 ± 0.08, Fig. 2A). Of all axon collaterals 79.2 ± 14.5% projected toward the pial surface (Fig. 2B,C), mostly terminating in L5 with a dense axonal plexus (example in Fig. 1B, density map in Fig. 3, all reconstructions in Supplementary Fig. 2B). L5-projecting interneurons preferentially innervated L5 of PFC: of all PFC L6 interneuron clusters, these neurons had the largest fraction of the axon residing in L5 (52.4 ± 18.0%, $P = 1.62E-12$ between all clusters, Table 1).

Morphological Cluster 3: Locally Projecting Interneurons

Cluster 3 of PFC L6 interneurons, termed locally projecting L6 interneurons consisted of 18 neurons, that is, 38% of the total number of interneurons (all reconstructions in Supplementary Fig. 3A). Axons of these interneurons were confined to their home layer with a distribution ratio of 88.3 ± 8.7%, a value significantly larger than that of all other clusters ($P = 1.16E-12$ between all clusters, Table 1 and Fig. 3). Locally projecting L6 interneurons were found in the middle of L6 with an average soma position of 0.35 ± 0.13; their axons showed no preferential projection toward superficial or deep cortical layers (45.4 ± 20.7% of the axons found between pia and soma while 54.6 ± 20.7% were located between soma-and WM, Fig. 2). This projection pattern suggests that locally projecting L6 interneurons mainly innervate a narrow stratum in their home layer.

Morphological Cluster 4: L6/WM-Projecting Interneurons

The last cluster, the L6/WM-projecting interneurons, comprised 10 cells and constituted 21% of the total number of interneurons in our study (all reconstructions in Supplementary Fig. 3B). Interneurons of this cluster displayed a dominant horizontal axonal projection compared with all other clusters (axon horizontal/vertical: 1.29 ± 0.43, $P = 0.006$ between all clusters, Table 1). They were found closer to the WM rather than the L5/L6 border (relative soma position: 0.63 ± 0.09, $P = 1.8E-09$ compared with all other clusters, Table 1 and Fig. 2A); therefore, they are mostly L6B interneurons: The axon collaterals of these neuron cluster projected preferentially toward the WM and less so to the pial surface (67.3 ± 17.8 vs. 32.7 ± 17.8, Fig. 2C). Unlike all other clusters, a significant proportion of the axon of cluster 4 L6 interneurons was located in the WM (26.8 ± 13.2%, $P = 2.12E-07$ when compared with all the other clusters, Table 1 and Fig. 3).

The axonal projection pattern of L6 interneurons in PFC was correlated with the position of the interneuron soma in L6 ($P = 0.0005$). Interneurons located at the L5/L6 border have axons that project preferentially to the pial surface with only few collaterals projecting to the WM (Fig. 2B). In contrast, neurons located close to the L6/WM border extended their axons predominately in the direction of the WM.

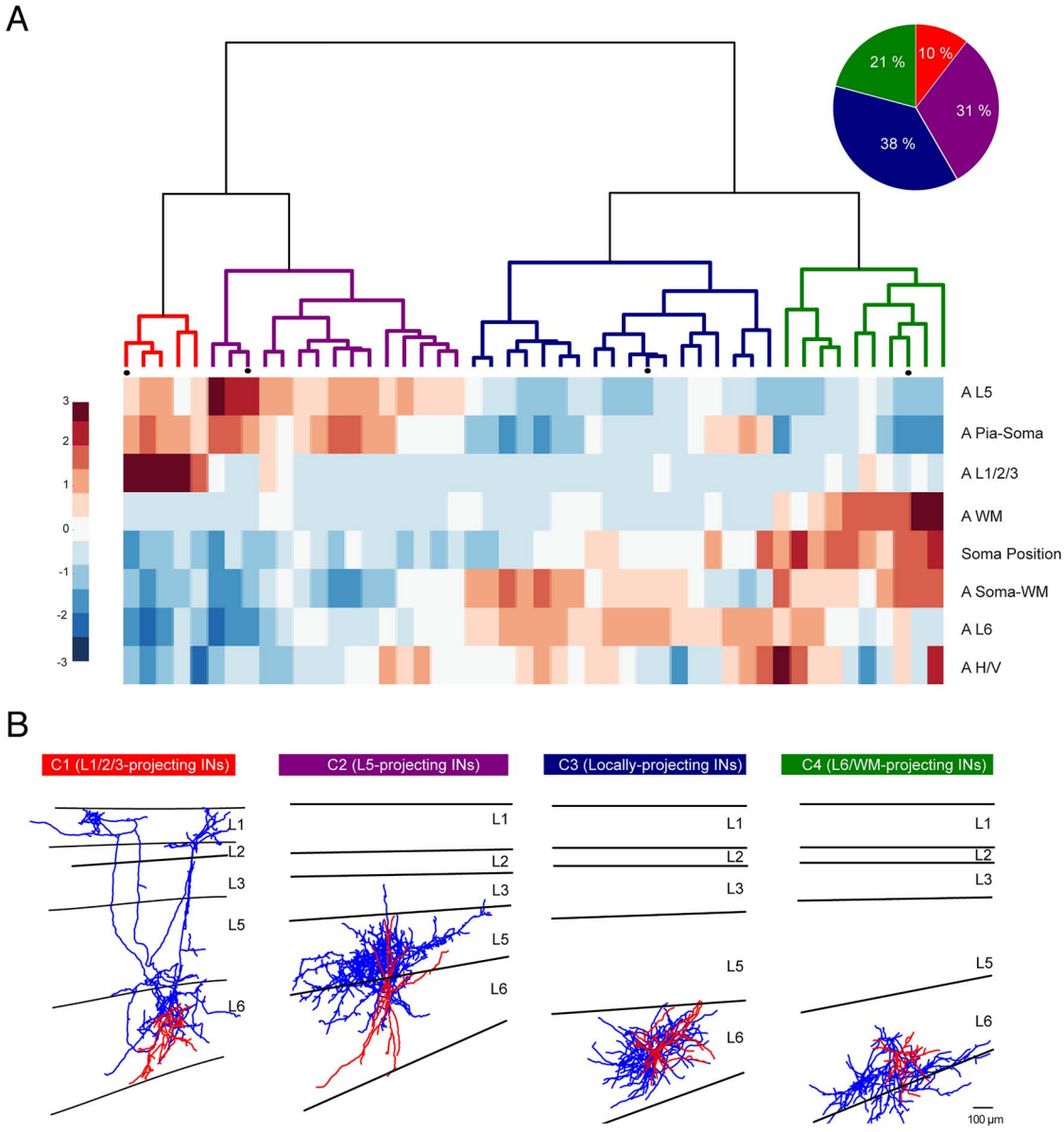

Figure 1. Morphological analysis of L6 inhibitory neurons using unsupervised cluster analysis. (A) Dendrogram obtained from a cluster analysis based on morphological parameters reveals four clusters of L6 interneurons ($n = 48$). The color map below the dendrogram indicates the standardized values of the corresponding parameters (listed on the right) of individual neurons, in which red represents values above the mean, white represents the mean, and blue represents values below the mean. Pie chart shows the percentage contribution of each cluster. (B) Representative axodendritic morphologies of the four clusters. Dendrites are shown in red and axons in blue. A L5: axonal distribution in L5; A Pia-Soma: axonal distribution from Pia-Soma; A L1/2/3: axonal distribution in L1-L3; A WM: axonal distribution in WM; A Soma-WM: axonal distribution from Soma-WM; Soma position: relative soma position in L6; A L6: axonal distribution in L6; A H/V: axon horizontal/vertical.

Correlation between Morphological and Electrophysiological Properties

Several studies have demonstrated that the axonal projection pattern of cortical interneurons and their intrinsic electrophysiological properties are—if at all—only weakly correlated so that a combination of electrophysiological and morphological parameters is often not helpful to classify interneurons (Gupta et al. 2000; Wang et al. 2002; Markram et al. 2004; Wang et al. 2004; Kumar and Ohana 2008; Helmstaedter et al. 2009; Arzt et al. 2018; Emmenegger et al. 2018; Feldmeyer et al. 2018). In this study, active electrical properties of interneurons of the different morphological clusters were determined and compared for different morphological clusters. Interneurons with a series resistance of >50 MΩ were excluded from this analysis. Therefore, in order to determine a correlation between electrophysiological and morphological parameters we used 5 neurons in morphological C1, 10 in C2, 11 in C3 and 9 in C4. Passive membrane properties were not included in this classification (Supplementary Table 2). PFC L6 interneurons could be categorized into several groups based on their firing behavior (Ascoli et al. 2008; Feldmeyer et al. 2018). Here, we found that L1/2/3-projecting interneurons were adapting

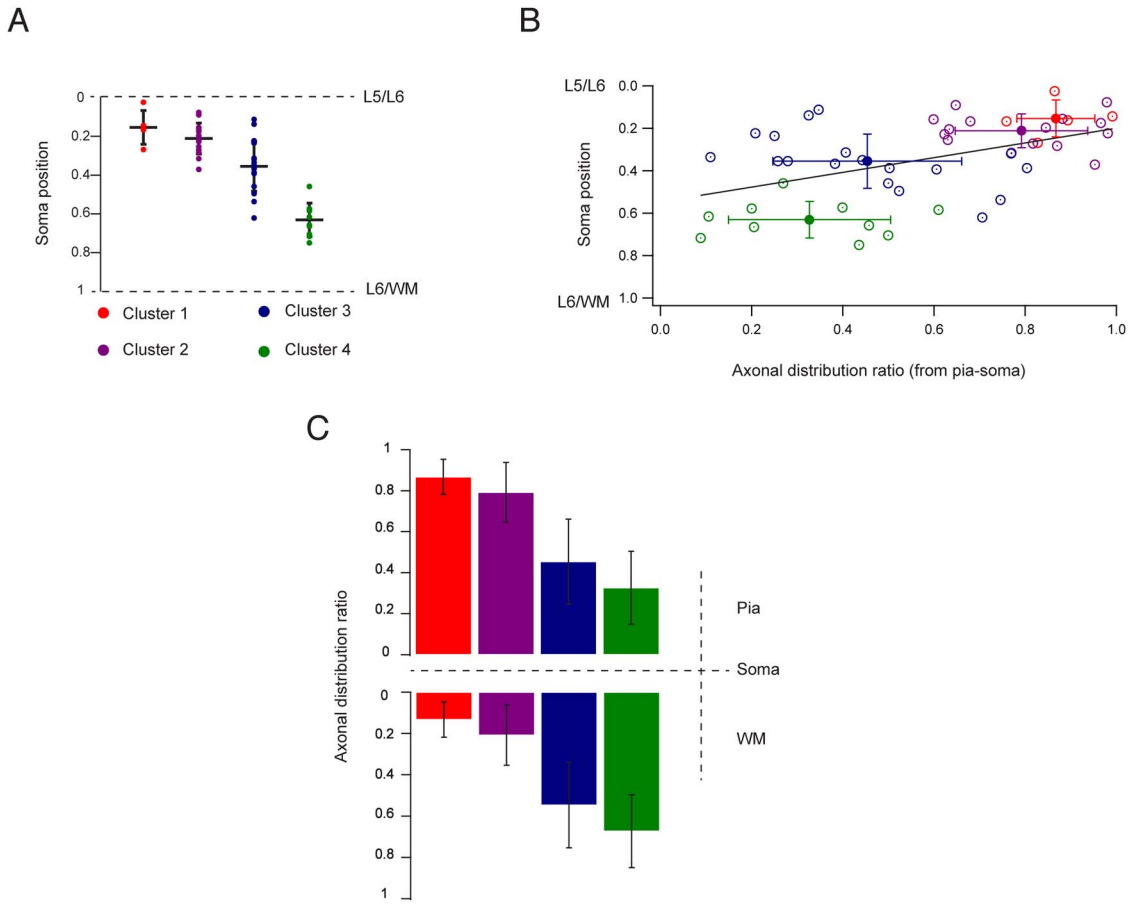

Figure 2. mPFC L6 interneurons display a strong correlation between soma position and axonal projection pattern. (*A*) Relative soma position in L6 of interneurons of the four morphological clusters. (*B*) Correlation between soma position of individual L6 interneurons and their axonal distribution from pia to soma. (*C*) Relative axonal distributions of the neurons from different clusters are shown. Top: from pia to soma; Bottom: from soma to WM.

neurons (example in Fig. 4A,B) with a significantly smaller adaptation ratio of 0.38 ± 0.24 (2nd ISI/10th ISI; P = 7.08E-04, Table 2, details of comparison in Fig. 4C) and a larger standard deviation of the ISI (34.1 ± 13.7 ms; P = 2.18E-04, Table 2, details of comparison in Fig. 4C) compared with interneurons of all other clusters. Moreover, the AP halfwidth of L1/2/3-projecting interneurons was much longer compared with interneurons in morphological clusters 2–4 (0.81 ± 0.16 ms; P = 0.001, Table 2, details of comparison in Fig. 4C). All L5-projecting interneurons displayed a fast-spiking (FS) firing pattern; eight of them displayed stuttering firing behavior, while the other seven showed continuous AP firing (examples in Fig. 4A,B). The ISI of L5-projecting interneurons was 26.0 ± 10.2 ms, which was the smallest among all four clusters (P = 0.008, Table 2, details of comparison in Fig. 4C). In addition, these L6 interneurons had also the largest AHP amplitude (25.2 ± 3.4 mV; P = 0.001, Table 2, details of comparison in Fig. 4C). Unlike interneurons in clusters 1 and 2, those in clusters 3 and 4 displayed heterogeneous firing patterns (but see below). Interneurons with FS, adapting and nonadapting non-FS firing behavior were found. To identify a possible correlation between axonal projecting pattern and AP firing properties, we performed a CA with the 35 interneurons with both morphological and electrophysiological properties that matched the criteria given above. The morphological and electrophysiological parameters used for the CA are listed in Fig. 5A. The combined CA revealed four clusters, —termed clusters A–D—which were largely similar to the morphological cluster 1–4 (Figs 1A and 5A). Cluster A consisted of 5 L1/2/3-projecting interneuron and one locally projecting (cluster 3) L6 interneuron. Cluster B comprised 11 interneuron, including all the L5-projecting interneurons and one locally projecting interneuron. Cluster C consisted of 9 locally projecting interneurons and one L6/WM-projecting interneuron, while the remainder of the L6/WM-projecting interneuron were placed in cluster D. A strong correlation between axonal morphology and active membrane properties was found for cluster A and B; for cluster C and D subclusters showing either a FS or a non-FS firing patterns were identified (Supplementary Fig. 4).

Neurochemical Expression of Interneurons in L6 of mPFC

To correlate the electrophysiological properties with the expression of neurochemical marker specific for different cortical interneuron types, we performed patch-clamp recordings with simultaneous filling of biocytin and the fluorescent dye Alexa 594 to allow an unambiguous identification of the recorded neuron. After determining the passive and active electrophysiological properties, slices were briefly fixed in PFA and processed for immunostaining for PV, SOM, and Prox1, a marker

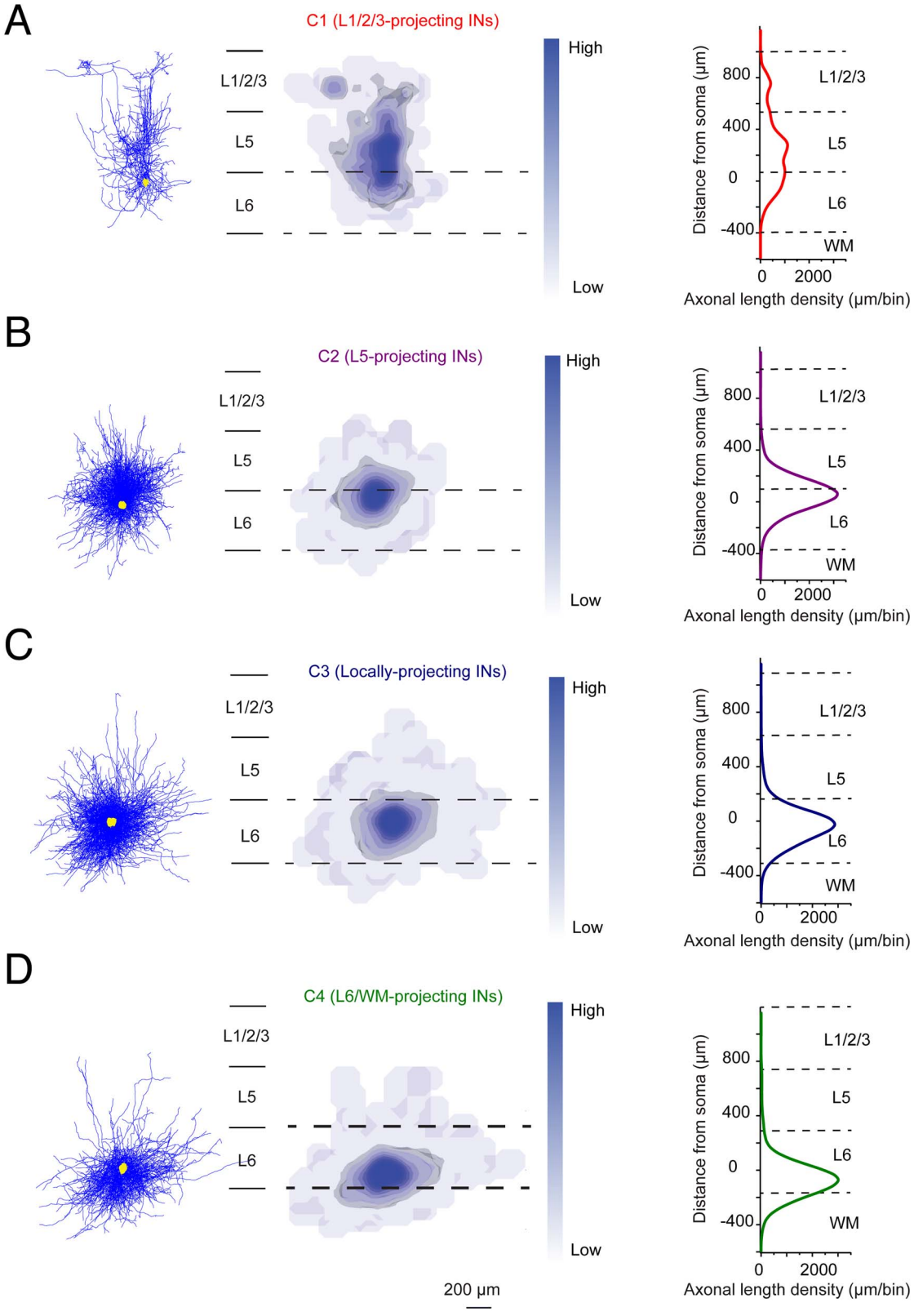

Figure 3. Reconstruction overlays and density maps of inhibitory mPFC L6 interneuron axons based on 4 morphological clusters. Left: All interneurons are aligned with their soma position represented as yellow dots; axons are shown in blue. Middle: 2D density maps of different clusters, the outer border of gray isosurfaces show the 80 percentile of the axonal density. Right: vertical axonal distribution of L6 interneuron clusters. The individual curves show the average axon density distribution along the vertical axis; bin size in the x axis: 50 μm in vertical direction. Dashed lines indicate layer borders. Results from 5 L1/2/3-projecting interneurons, 15 L5-projecting interneurons, 18 locally projecting L6 interneurons, and 10 L6/WM-projecting interneurons are shown in panel A, B, C, and D, respectively.

Table 2 Statistical analysis of the electrophysiological parameters under 4 morphological clusters

Parameters	C1	C2	C3	C4	P value
ISI average (ms)	74.5 ± 6.1	26.0 ± 10.2	37.3 ± 21.9	53.7 ± 27.8	0.008
ISI SD (ms)	34.1 ± 13.7	2.3 ± 2.0	8.3 ± 11.0	6.4 ± 4.7	2.18E-04
AP half-width (ms)	0.81 ± 0.16	0.42 ± 0.12	0.58 ± 0.17	0.51 ± 0.18	1.45E-03
AP threshold (mV)	−37.9 ± 1.9	−30.6 ± 6.2	−32.2 ± 7.5	−33.7 ± 3.3	0.04
AHP amplitude (mV)	16.3 ± 4.2	25.2 ± 3.4	19.1 ± 4.2	21.4 ± 2.9	1.22E-03
Adaptation ratio	0.38 ± 0.24	0.91 ± 0.12	0.66 ± 0.25	0.83 ± 0.09	7.08E-04
Firing frequency (Hz)/100 pA	24.1 ± 6.3	36.7 ± 14.9	30.8 ± 21.1	32.5 ± 14.4	0.39

All data are represented as mean ± standard deviation. The Kruskal–Wallis test was used to test for significant differences between clusters.

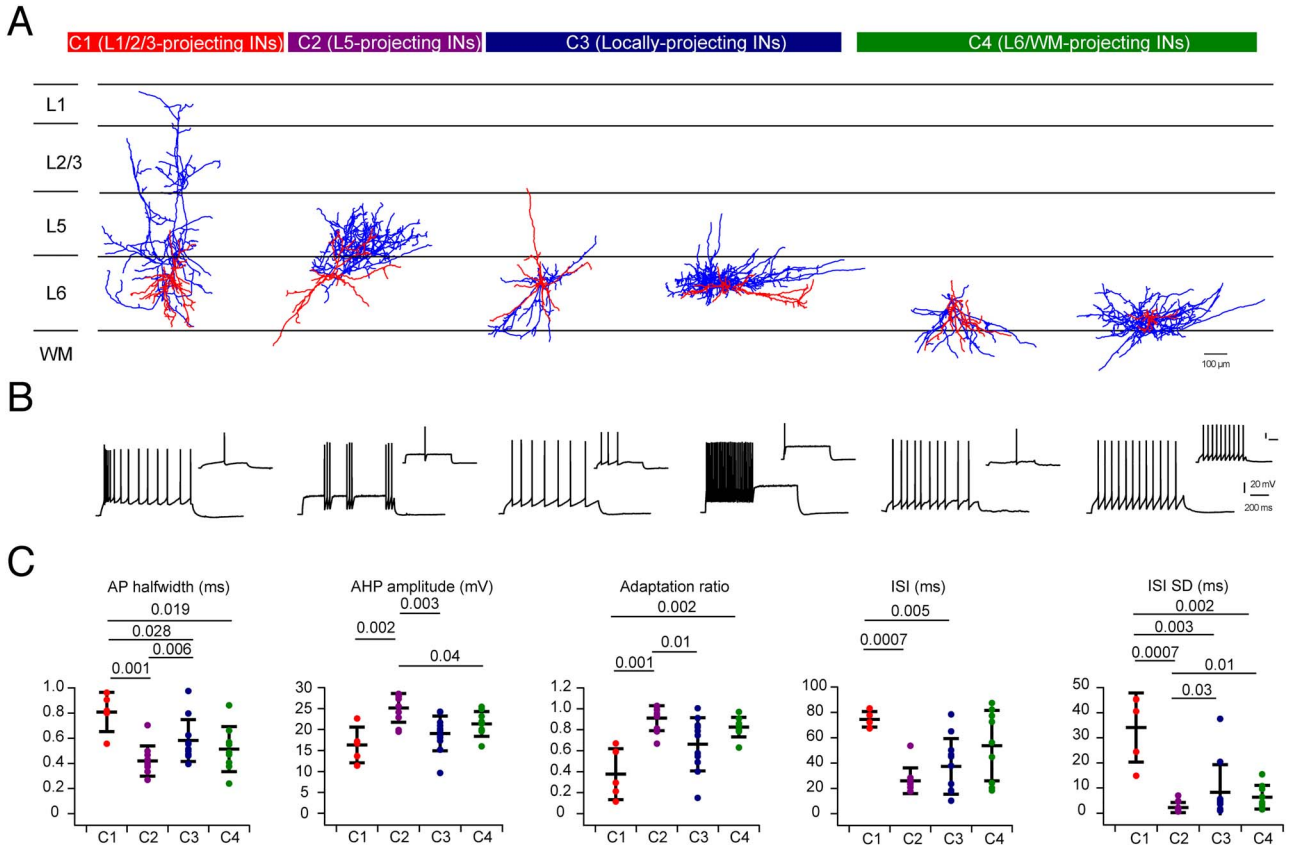

Figure 4. Comparison of electrophysiological parameters in morphological clusters of L6 interneurons in rat mPFC. (*A*) Representative examples of L6 interneurons of the four morphological clusters. Axons are given in blue, the somatodendritic domain in red. (*B*) Corresponding firing pattern of the neurons that are shown in A (10-spike train and the first AP at rheobase current injection). (*C*) Statistical analysis of the active electrophysiological properties of mPFC L6 interneurons in the four morphological clusters. A Wilcoxon–Mann–Whitney test was performed for the significant difference among clusters. *P* values are shown above these two clusters (examples in *A* and *B*).

for vasoactive intestinal peptide-expressing interneurons (Saha et al. 2016) and a fraction of reelin-and calretinin-expressing interneurons (Rubin and Kessaris 2013; Miyoshi et al. 2015) (the expression of these markers in different mPFC layers is shown in Supplementary Fig. 5). A subsequent DAB staining of the slices was made to determine the morphology of the labeled neurons. Of 17 PFC L6 interneurons, seven were PV-positive, four SOM-positive and five Prox1-positive. One interneuron showed no immunoreactivity for any of the three neurochemical markers. After analyzing the active firing pattern of the labeled interneurons, we found that in accordance with previous findings, PV-positive neurons were always FS interneurons, with either continuous or stuttering spiking. SOM-positive and Prox1-positive interneurons were all non-FS interneurons; they displayed heterogeneous firing patterns with both adapting and nonadapting non-FS behaviors (examples in Fig. 6).

Discussion

Here we identified four distinct clusters of interneurons in layer 6 of the mPFC, which can be distinguished based on their axonal projection pattern (Fig. 7). Similar to L6 pyramidal cells in the rat mPFC (van Aerde and Feldmeyer 2015), L6 interneurons showed a high degree of morphological diversity, ranging from small neurons that were exclusively confined to their home layer to neurons with axons projecting to either superficial layers terminating in L1 or deep in the white matter.

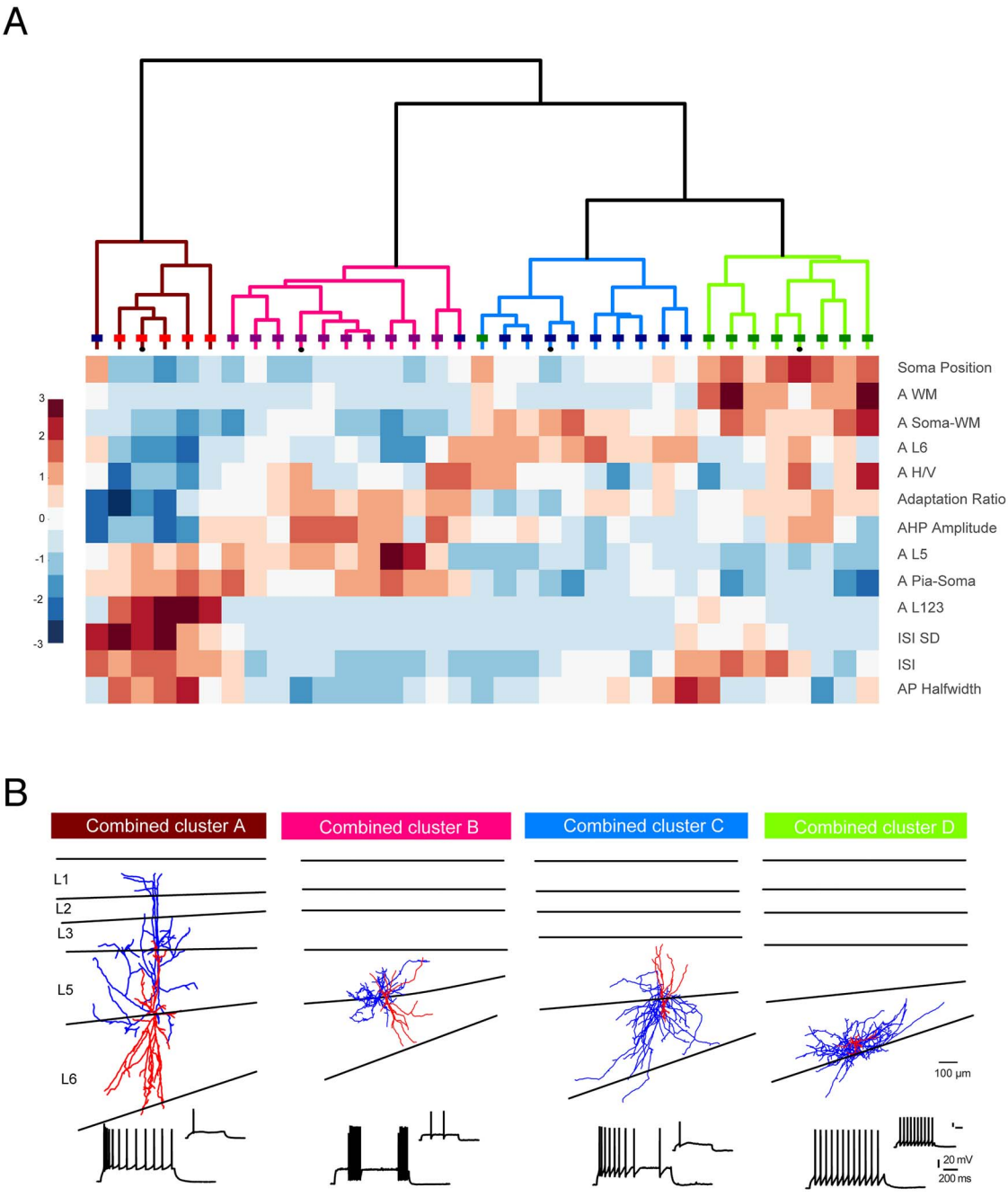

Figure 5. Comparison of morphological and electrophysiological parameters of L6 interneurons in rat mPFC. (*A*) A combined unsupervised hierarchical cluster analysis based on both morphological and electrophysiological parameters revealed four clusters. The cut-off for significant clusters is 70% of the maximum linkage distance. Colored lines in each dendrogram represent the color code from the morphological clusters in (*B*). Colored boxes on each line show the morphology clusters the neurons belong to. The color map below the dendrogram indicates the standardized values of the corresponding parameters (listed on the right) of individual neurons, in which red represents values above the mean, white represents the mean, and blue represents values below the mean (see Fig. 1). (*B*) Representative examples of L6 inhibitory neurons based on combined morphological/electrophysiological parameters. Axons are given in blue, the somatodendritic domains in red. Corresponding firing pattern are shown below each example morphology.

Classification of Interneurons in Layer 6 of Different Cortical Areas

Using classification methods (CA based on the axonal properties) similar to those used in our previous work, a study in somatosensory barrel cortex identified five independent groups, including interneurons with local or translaminar axonal projection (Arzt et al. 2018). The L6 interneuron types identified in that study showed only a partial overlap with those described here. In particular, the "L2/3/4 inhibitors" and "L5b inhibitors" of that study resembled the L1/2/3-projecting and L5-projecting interneurons in PFC, respectively. L5-projecting, FS PV-positive L6 interneurons have also been identified in rat visual cortex and

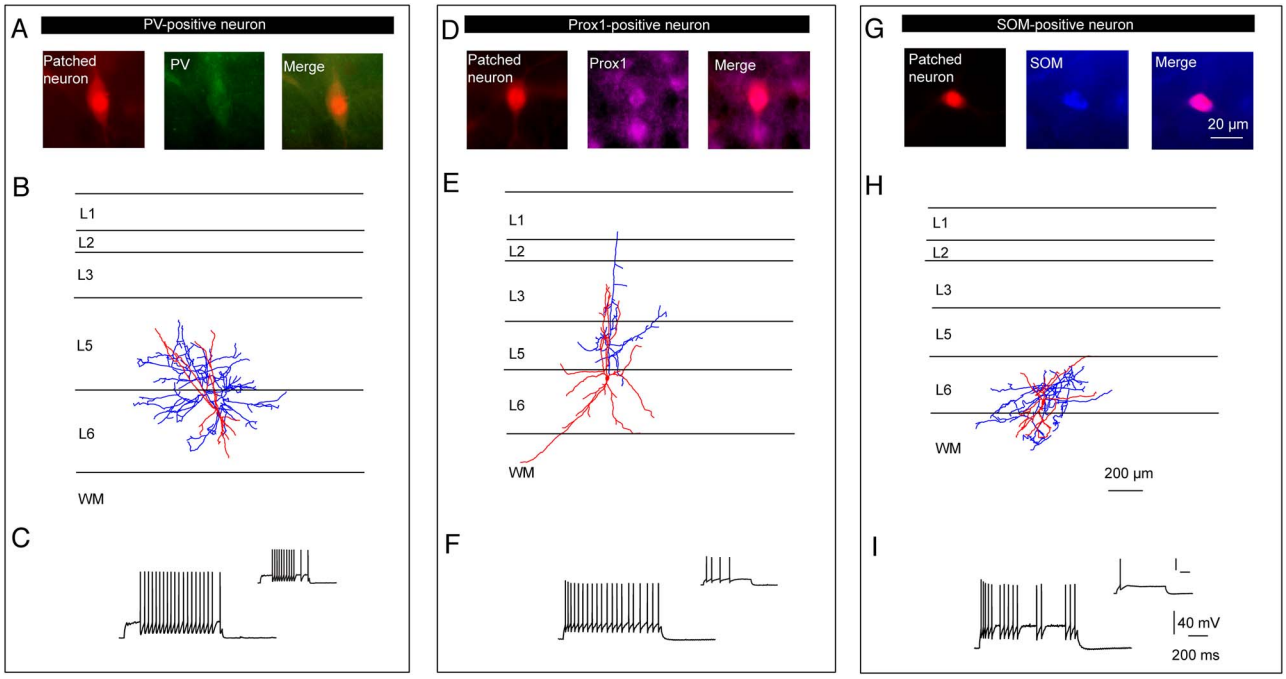

Figure 6. Neurochemical marker expression of individual L6 interneurons in rat mPFC. Whole-cell patch-clamp recordings were made with simultaneous biocytin and Alexa 594 filling (red) to identify the location of patched neurons. Immunostaining was performed after a brief fixation period in PFA to check the expression of PV (green), Prox1 (purple), and SOM (blue) of the patched neurons. Representative examples of interneurons expressing PV (*A*), Prox1 (*D*), and somatostatin (*G*) with morphological reconstructions (*B*, *E*, *H*) and firing pattern (*C*, *F*, *I*, left: the first 10 spikes traces; right: the firing traces at the current 100 pA above the threshold) are shown. Axon is labeled in blue, soma and dendrites in red.

are predominantly innervated by corticothalamic L6 pyramidal cells (West et al. 2006).

The interneuron type coined locally (L6)-projecting interneurons here includes the L6, L5/6 and L6/5 inhibitors and comprises both FS and non-FS interneurons; this may therefore be a less well-defined class of L6 interneurons comprising several distinct structural and functional types. A PFC locally projecting L6 interneuron type has also been identified in rodent barrel cortex and showed a FS pattern and PV expression (Kumar and Ohana 2008; Frandolig et al. 2019); therefore, these interneurons can be described as small or large L6 basket cells. So-called translaminar "L4-targeting L6 inhibitory neurons" were also identified in these studies (Kumar and Ohana 2008; Tan et al. 2008; Frandolig et al. 2019) which have no correspondence to a L6 interneuron type described here because rodent PFC lacks a distinct layer 4. The L6/WM-projecting interneuron group was, however, not found in any previous study of rat barrel cortex L6 interneurons.

In another study on L6 interneurons in barrel cortex (Perrenoud et al. 2013), the authors identified four different types of interneurons mainly based on AP firing properties and molecular marker expression. The axonal domain of these interneurons was not analyzed quantitatively, making it difficult to compare the L6 interneuron types of that study directly with those found here. Similar to our findings, the authors found that ~50% of all L6 interneurons were FS, PV-expressing putative L6 small and large basket cells while the remainder were non-FS, adapting firing interneurons expressing neuropeptide Y, SOM and vasoactive intestinal peptide (Saha et al. 2016), respectively.

In a recent study using a correlated analysis of electrophysiological, molecular/transcriptomic and morphological properties of interneurons in mouse visual cortex, several distinct neuronal cell types were identified (Gouwens et al. 2019). Using single-cell RNA sequencing, the authors describe three subsets of L6 interneurons most of which have a local axonal domain. They did not describe a group of L1/2/3-projecting L6 interneurons although they show a single example of a SOM-positive L6 interneuron that projects to layers 1 and 2/3 in their publication. PFC L6 interneurons in cluster 2 resemble to some extent the PV-expressing interneurons described by Gouwens et al. (2019), which can be tentatively described as large basket cells. However, a subset of the PV interneurons of that study is located in L6B and appears to be similar to the PFC FS interneurons in clusters 3 and 4. In a follow-up study three different transcriptomic types of PV-expressing interneurons were identified in L6 (Hodge et al. 2019). One group of L6 interneurons in visual cortex termed "wide axon, small dendrites" interneurons showed a high degree of similarity with the majority of the cluster 4 L6/WM-projecting interneurons identified here. In visual cortex these interneurons express the lysosomal-associated membrane protein 5 (Lamp5) and are presumably L6 neurogliaform cells (Hodge et al. 2019). The classification based on transcriptomic features is apparently better correlated with electrophysiological properties than with neuronal morphology, consistent with a single-cell PCR study in mouse barrel cortex (Perrenoud et al. 2013).

Correlation between Interneuron Types and Electrophysiological Properties

The electrophysiological properties of PFC L6 interneurons are very heterogeneous, in accordance with findings in other brain regions (Kawaguchi 1993; Cauli et al. 1997; Ascoli et al. 2008; DeFelipe et al. 2013; Feldmeyer et al. 2018). We found

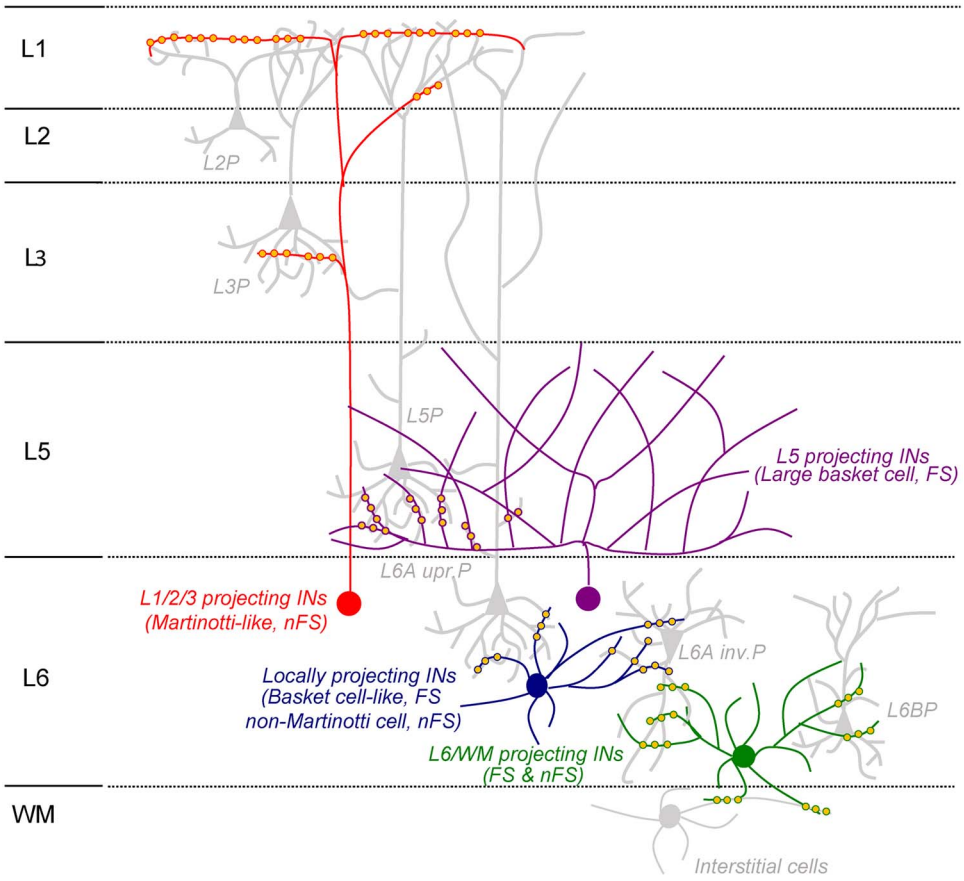

Figure 7. Schematic summary of the potential targets of the four types of interneurons in L6 of mPFC. P: pyramidal cells; upr. P: upright pyramidal cells; inv. P: inverted pyramidal cells. L1/2/3 projecting interneurons (red) are, in our study, Martinotti-like interneurons projecting mainly to the superficial layers and potentially targeting distal dendrites of excitatory neurons from different layers. L5-projecting interneurons (purple) are mostly FS interneurons and they potentially inhibit L5 basal dendrites of excitatory neurons and L6 upright pyramidal cells. Locally projecting interneurons (blue) are more like basket cells, potentially targeting basal dendrites of different L6 excitatory neurons. The last type, L6/WM-projecting interneurons (green), is located in the deep L6 and preferentially targets WM. Potential synaptic connections are labeled as small puncta (yellow filling) in different layers.

no correlation between the axonal projection of PFC L6 interneurons and their passive membrane properties; however, for the L1/2/3- and L5-projecting L6 interneurons the firing pattern and morphology show some degree of correlation: all L1/2/3-projecting interneurons exhibited adapting AP firing while all L5-projecting interneurons were FS interneurons, as found in visual cortex (West et al. 2006). Locally and L6/WM-projecting interneurons showed disparate firing patterns and the combined morphological-electrophysiological CA revealed subgroups in these two clusters. Both locally and L6/WM-projecting PFC L6 interneurons can be subdivided into FS and non-FS interneurons (Supplementary Fig. 4). Notably, only non-FS but not FS L6/WM-projecting interneurons have a single axon branch that extend to L2/3 (Supplementary Fig. 4E) suggesting that electrophysiological parameters may help to reveal the existence of interneuron subtypes.

Differential Innervation of mPFC Neurons by L6 Interneurons

Interneurons in mPFC receive synaptic input predominantly from adjacent and granular frontal cortical regions but also from virtually all other regions of the isocortex, for example, motor, sensory, and associative cortices (Pandya and Yeterian 1990; Petrides and Pandya 1999; Ahrlund-Richter et al. 2019; Sun et al. 2019). In L6, interneurons also receive direct thalamocortical input (Beierlein and Connors 2002). Furthermore, in visual cortex corticothalamic L6 pyramidal cells have been suggested to innervate L6 interneurons with a higher connection probability than corticocortical cells (West et al. 2006). However, the axonal properties and innervation domains of mPFC L6 interneurons have so far not been described quantitatively.

L1/2/3-Projecting Interneurons

This group of interneurons is the smallest population of our sample of 48 interneurons, a finding similar to that for L6 somatosensory cortex (Arzt et al. 2018). They target preferentially superficial layers, resembling SOM-expressing Martinotti-like neurons (Fairén et al. 1984; Kawaguchi and Kubota 1997; Wang et al. 2004). A distinctive feature of these putative PFC L6 "Martinotti cells" is that they only sparsely innervate their home layer; most of their axon collaterals reside in superficial layers, projecting in a largely vertical fashion; they form only little if any synaptic connections within their home layer, but establish inhibitory connections with the apical dendritic tufts of PFC pyramidal cells (Silberberg and Markram 2007; Murayama

et al. 2009; Higley 2014; Yavorska and Wehr 2016). This dendritic compartment of pyramidal cells is near the initiation zone for NMDA and Ca^{2+} spikes (Larkum et al. 1999; Palmer et al. 2014), the generation of which can be effectively inhibited by the L1/2/3-projecting L6 interneurons. This may lead to a block of the association of synaptic inputs arriving in the PFC in different cortical layers. This is particularly valid for the broad-tufted pyramidal cells in layer 2 (100% of all L2 pyramidal cells), layer 3 (55%) and layer 5 (27%) (van Aerde and Feldmeyer 2015).

Some of the L1/2/3-projecting L6 interneurons may also belong to the rare group of L6 VIP cells which do not appear to have the typical bipolar morphology of VIP cells in L2/3 (Perrenoud et al. 2013; Pronneke et al. 2015) but here we did not find VIP-positive L1/2/3-projecting interneurons in layer 6 of the PFC.

L5-Projecting Interneurons

As found for L1/2/3-projecting interneurons, this cluster of neurons mainly targets neurons outside the home layer with most of their axonal collaterals located in L5. It is therefore likely that these neurons target the basal dendrites of pyramidal cells in L5 and in particular L5B. They may also innervate the proximal portion of the apical dendrites of L6 upright pyramidal cells. The axonal projection pattern of L5-projecting interneurons were similar to those of the "L5b inhibitors" found in L6 of somatosensory cortex (Arzt et al. 2018). L5-projecting interneurons may play an important role in determining spike timing during slow oscillation episodes (van Aerde et al. 2009).

Together with the locally projecting L6 interneurons, L5-projecting interneurons may also control the effect of dopaminergic input to PFC L5 and L6 pyramidal cells. The density of dopaminergic afferents and postsynaptic dopamine receptors is highest in layers 5 and 6 of the PFC and other cortical areas (Weiner et al. 1991; Gaspar et al. 1995; Santana and Artigas 2017).

Locally Projecting Interneurons

These mPFC L6 interneurons are located close to the middle portion of L6 and are likely to establish synaptic contacts mainly with basal dendrites of upright pyramidal cells, as well as main and basal dendrites of inverted pyramidal cells. In somatosensory barrel cortex, these excitatory neuron types have a wide axonal plexus (Zhang and Deschenes 1997; Pichon et al. 2012; Narayanan et al. 2015) that is likely to relay cortical excitation to both superficial cortical layers and distal cortical areas, thereby distributing thalamic input. In the barrel cortex, locally projecting L6 FS interneurons are strongly innervated by thalamic afferents (Frandolig et al. 2019) and are thus in a position to integrate local and thalamocortical inputs, thereby controlling both intracortical and subcortical (mostly thalamic) synaptic signaling of excitatory L6 pyramidal cells (for PFC see e.g., Gabbott et al. 2005; for barrel cortex see e.g., Pichon et al. 2012).

They may also target other PFC L6 interneurons, thus forming disinhibitory microcircuits as described for locally projecting L1 and L2/3 interneurons (Jiang et al. 2013; Lee et al. 2015). In our hands, locally projecting L6 interneurons were not exclusively FS interneurons but showed also non-FS firing patterns. Based on their morphological features, locally projecting FS L6 interneurons are reminiscent of FS basket cells while locally projecting non-FS L6 interneurons could be the radially projecting neurogliaform-like cells (Kawaguchi and Kubota 1993; Wang et al. 2002; Armstrong et al. 2012; Overstreet-Wadiche and McBain 2015; Lagler et al. 2016; Gouwens et al. 2019).

L6/WM-Projecting Interneurons

The last group of L6 interneurons is located in deep layer 6 (i.e., layer 6B) and has extensive axonal projections in its home layer and the WM. Potential targets of L6/WM-projecting interneurons are basal dendrites of all L6B neurons as well as the "main" dendrites of L6B nonpyramidal excitatory neurons (Marx and Feldmeyer 2013; Gouwens et al. 2019). In addition, they may also form synaptic contacts with WM interstitial cells. These cells are considered to be among the oldest neurons of the cerebral cortex and remnants of the earliest generated subplate neurons; their density declines during development due to differential growth of the WM and an absolute decrease in subplate neuron number (Chun and Shatz 1989). It has been suggested that persistent WM interstitial cells receive excitatory and inhibitory input from cortical and subcortical areas and may form neuronal microcircuits that interact with subcortical signal transfer (von Engelhardt et al. 2011; see also Colombo 2018). L6/WM-projecting interneurons may be part of such microcircuits.

In this work we have attempted a first description of the interneuron complement of L6 of the mPFC, one of the major corticothalamic output layers which is involved in attention processes. The specific role played by these interneurons in the function of an associative cortex remains uncharted territory and further quantitative studies regarding the excitatory and inhibitory neuronal cell types and their dendritic and axonal projection patterns may reveal differences in the synaptic connectivity patterns of the mPFC and other cortical areas. This may help to elucidate structural differences between association and sensory cortices and their functional implications.

Supplementary Material

Supplementary material can be found at *Cerebral Cortex* online.

Notes

We thank Werner Hucko for excellent technical assistance and Dr Karlijn van Aerde for custom-written macros in Igor Pro software. We warmly thank Dr Guanxiao Qi and Dr Danqing Yang for helpful discussions. *Conflict of Interest*: The authors declare no conflicts of interest.

Funding

Helmholtz Society, European Union's Horizon 2020 Research, Innovation Programme (Grant Agreement No. 785907 (HBP SGA2) to D.F.); China Scholarship Council (to C.D.).

Author Contributions

D.F. conceived the research; D.F., C.D., and V.E. designed the experimental approach; C.D., V.E., and K.S. performed experiments and data analysis; C.D., V.E., and D.F. wrote the manuscript.

References

Ahrlund-Richter S, Xuan Y, van Lunteren JA, Kim H, Ortiz C, Pollak Dorocic I, Meletis K, Carlen M. 2019. A whole-brain atlas of monosynaptic input targeting four different cell types in the medial prefrontal cortex of the mouse. *Nat Neurosci*. 22:657–668.

Armstrong C, Krook-Magnuson E, Soltesz I. 2012. Neurogliaform and ivy cells: a major family of nNOS expressing GABAergic neurons. *Front Neural Circuit*. 6:23.

Arzt M, Sakmann B, Meyer HS. 2018. Anatomical correlates of local, Translaminar, and Transcolumnar inhibition by layer 6 GABAergic interneurons in somatosensory cortex. *Cereb Cortex*. 28:2763–2774.

Ascoli GA, Alonso-Nanclares L, Anderson SA, Barrionuevo G, Benavides-Piccione R, Burkhalter A, Buzsaki G, Cauli B, Defelipe J, Fairen A *et al*. 2008. Petilla terminology: nomenclature of features of GABAergic interneurons of the cerebral cortex. *Nat Rev Neurosci*. 9:557–568.

Beierlein M, Connors BW. 2002. Short-term dynamics of thalamocortical and intracortical synapses onto layer 6 neurons in neocortex. *J Neurophysiol*. 88:1924–1932.

Benes FM, Berretta S. 2001. GABAergic interneurons: implications for understanding schizophrenia and bipolar disorder. *Neuropsychopharmacology*. 25:1–27.

Beneyto M, Abbott A, Hashimoto T, Lewis DA. 2011. Lamina-specific alterations in cortical GABA(a) receptor subunit expression in schizophrenia. *Cereb Cortex*. 21:999–1011.

Brown VJ, Bowman EM. 2002. Rodent models of prefrontal cortical function. *Trends Neurosci*. 25:340–343.

Cauli B, Audinat E, Lambolez B, Angulo MC, Ropert N, Tsuzuki K, Hestrin S, Rossier J. 1997. Molecular and physiological diversity of cortical nonpyramidal cells. *J Neurosci*. 17: 3894–3906.

Chun JJ, Shatz CJ. 1989. Interstitial cells of the adult neocortical white matter are the remnant of the early generated subplate neuron population. *J Comp Neurol*. 282: 555–569.

Collins DP, Anastasiades PG, Marlin JJ, Carter AG. 2018. Reciprocal circuits linking the prefrontal cortex with dorsal and ventral thalamic nuclei. *Neuron*. 98:366–379 e364.

Colombo JA. 2018. Cellular complexity in subcortical white matter: a distributed control circuit? *Brain Struct Funct*. 223:981–985.

Connors BW, Gutnick MJ. 1990. Intrinsic firing patterns of diverse neocortical neurons. *Trends Neurosci*. 13:99–104.

DeFelipe J, Lopez-Cruz PL, Benavides-Piccione R, Bielza C, Larranaga P, Anderson S, Burkhalter A, Cauli B, Fairen A, Feldmeyer D *et al*. 2013. New insights into the classification and nomenclature of cortical GABAergic interneurons. *Nat Rev Neurosci*. 14:202–216.

Elston GN. 2003. Cortex, cognition and the cell: new insights into the pyramidal neuron and prefrontal function. *Cereb Cortex*. 13:1124–1138.

Emmenegger V, Qi G, Wang H, Feldmeyer D. 2018. Morphological and functional characterization of non-fast-spiking GABAergic interneurons in layer 4 microcircuitry of rat barrel cortex. *Cereb Cortex*. 28:1439–1457.

Euston DR, Gruber AJ, McNaughton BL. 2012. The role of medial prefrontal cortex in memory and decision making. *Neuron*. 76:1057–1070.

Fairén A, DeFelipe J, Regidor J. 1984. Nonpyramidal neurons. In: *Cerebral Cortex: Cellular Components of the Cerebral Cortex*, Peters A and Jones EG (eds.). New York: Plenum Press, pp. 206–211.

Feldmeyer D, Qi G, Emmenegger V, Staiger JF. 2018. Inhibitory interneurons and their circuit motifs in the many layers of the barrel cortex. *Neuroscience*. 368:132–151.

Frandolig JE, Matney CJ, Lee K, Kim J, Chevee M, Kim SJ, Bickert AA, Brown SP. 2019. The synaptic organization of layer 6 circuits reveals inhibition as a major output of a neocortical sublamina. *Cell Rep*. 28:3131–3143 e3135.

Fuster JM. 2001. The prefrontal cortex–an update: time is of the essence. *Neuron*. 30:319–333.

Fuster JM. 2015. *The Prefrontal Cortex*. Amsterdam: Boston: Elsevier/AP, Academic Press is an imprint of Elsevier.

Gabbott PL, Bacon SJ. 1996. Local circuit neurons in the medial prefrontal cortex (areas 24a,b,c, 25 and 32) in the monkey: I. cell morphology and morphometrics. *J Comp Neurol*. 364:567–608.

Gabbott PL, Bacon SJ. 1997. Vasoactive intestinal polypeptide containing neurones in monkey medial prefrontal cortex (mPFC): colocalisation with calretinin. *Brain Res*. 744: 179–184.

Gabbott PL, Dickie BG, Vaid RR, Headlam AJ, Bacon SJ. 1997. Local-circuit neurones in the medial prefrontal cortex (areas 25, 32 and 24b) in the rat: morphology and quantitative distribution. *J Comp Neurol*. 377:465–499.

Gabbott PL, Warner TA, Jays PR, Salway P, Busby SJ. 2005. Prefrontal cortex in the rat: projections to subcortical autonomic, motor, and limbic centers. *J Comp Neurol*. 492:145–177.

Gaspar P, Bloch B, Le Moine C. 1995. D1 and D2 receptor gene expression in the rat frontal cortex: cellular localization in different classes of efferent neurons. *Eur J Neurosci*. 7:1050–1063.

Gouwens NW, Sorensen SA, Berg J, Lee C, Jarsky T, Ting J, Sunkin SM, Feng D, Anastassiou CA, Barkan E *et al*. 2019. Classification of electrophysiological and morphological neuron types in the mouse visual cortex. *Nat Neurosci*. 22:1182–1195.

Guillery RW, Sherman SM. 2002. Thalamic relay functions and their role in corticocortical communication: generalizations from the visual system. *Neuron*. 33:163–175.

Gupta A, Wang Y, Markram H. 2000. Organizing principles for a diversity of GABAergic interneurons and synapses in the neocortex. *Science*. 287:273–278.

Helmstaedter M, Sakmann B, Feldmeyer D. 2009. The relation between dendritic geometry, electrical excitability, and axonal projections of L2/3 interneurons in rat barrel cortex. *Cereb Cortex*. 19:938–950.

Higley MJ. 2014. Localized GABAergic inhibition of dendritic Ca(2+) signalling. *Nat Rev Neurosci*. 15:567–572.

Hirai Y, Morishima M, Karube F, Kawaguchi Y. 2012. Specialized cortical subnetworks differentially connect frontal cortex to parahippocampal areas. *J Neurosci*. 32:1898–1913.

Hiser J, Koenigs M. 2018. The multifaceted role of the ventromedial prefrontal cortex in emotion, decision making, social cognition, and psychopathology. *Biol Psychiatry*. 83: 638–647.

Hodge RD, Bakken TE, Miller JA, Smith KA, Barkan ER, Graybuck LT, Close JL, Long B, Johansen N, Penn O *et al*. 2019. Conserved cell types with divergent features in human versus mouse cortex. *Nature*. 573:61–68.

Jiang X, Wang G, Lee AJ, Stornetta RL, Zhu JJ. 2013. The organization of two new cortical interneuronal circuits. *Nat Neurosci*. 16:210–218.

Kawaguchi Y. 1993. Physiological, morphological, and histochemical characterization of three classes of interneurons in rat neostriatum. *J Neurosci*. 13:4908–4923.

Kawaguchi Y, Kubota Y. 1993. Correlation of physiological subgroupings of nonpyramidal cells with parvalbumin- and calbindinD28k-immunoreactive neurons in layer V of rat frontal cortex. *J Neurophysiol*. 70:387–396.

Kawaguchi Y, Kubota Y. 1997. GABAergic cell subtypes and their synaptic connections in rat frontal cortex. *Cereb Cortex*. 7:476–486.

Kepecs A, Fishell G. 2014. Interneuron cell types are fit to function. *Nature*. 505:318–326.

Krettek JE, Price JL. 1977. The cortical projections of the mediodorsal nucleus and adjacent thalamic nuclei in the rat. *J Comp Neurol*. 171:157–191.

Krimer LS, Goldman-Rakic PS. 2001. Prefrontal microcircuits: membrane properties and excitatory input of local, medium, and wide arbor interneurons. *J Neurosci*. 21:3788–3796.

Krimer LS, Zaitsev AV, Czanner G, Kroner S, Gonzalez-Burgos G, Povysheva NV, Iyengar S, Barrionuevo G, Lewis DA. 2005. Cluster analysis-based physiological classification and morphological properties of inhibitory neurons in layers 2-3 of monkey dorsolateral prefrontal cortex. *J Neurophysiol*. 94:3009–3022.

Kubota Y, Hatada S, Kondo S, Karube F, Kawaguchi Y. 2007. Neocortical inhibitory terminals innervate dendritic spines targeted by thalamocortical afferents. *J Neurosci*. 27:1139–1150.

Kumar P, Ohana O. 2008. Inter- and intralaminar subcircuits of excitatory and inhibitory neurons in layer 6a of the rat barrel cortex. *J Neurophysiol*. 100:1909–1922.

Lagler M, Ozdemir AT, Lagoun S, Malagon-Vina H, Borhegyi Z, Hauer R, Jelem A, Klausberger T. 2016. Divisions of identified parvalbumin-expressing basket cells during working memory-guided decision making. *Neuron*. 91:1390–1401.

Larkum M. 2013. A cellular mechanism for cortical associations: an organizing principle for the cerebral cortex. *Trends Neurosci*. 36:141–151.

Larkum ME, Waters J, Sakmann B, Helmchen F. 2007. Dendritic spikes in apical dendrites of neocortical layer 2/3 pyramidal neurons. *J Neurosci*. 27:8999–9008.

Larkum ME, Zhu JJ, Sakmann B. 1999. A new cellular mechanism for coupling inputs arriving at different cortical layers. *Nature*. 398:338–341.

Ledergerber D, Larkum ME. 2010. Properties of layer 6 pyramidal neuron apical dendrites. *J Neurosci*. 30:13031–13044.

Lee AJ, Wang G, Jiang X, Johnson SM, Hoang ET, Lante F, Stornetta RL, Beenhakker MP, Shen Y, Julius Zhu J. 2015. Canonical organization of layer 1 neuron-led cortical inhibitory and disinhibitory interneuronal circuits. *Cereb Cortex*. 25: 2114–2126.

Lein ES, Belgard TG, Hawrylycz M, Molnar Z. 2017. Transcriptomic perspectives on neocortical structure, development, evolution, and disease. *Annu Rev Neurosci*. 40:629–652.

Leonard CM. 2016. Finding prefrontal cortex in the rat. *Brain Res*. 1645:1–3.

Lubke J, Roth A, Feldmeyer D, Sakmann B. 2003. Morphometric analysis of the columnar innervation domain of neurons connecting layer 4 and layer 2/3 of juvenile rat barrel cortex. *Cereb Cortex*. 13:1051–1063.

Markram H, Toledo-Rodriguez M, Wang Y, Gupta A, Silberberg G, Wu C. 2004. Interneurons of the neocortical inhibitory system. *Nat Rev Neurosci*. 5:793–807.

Marx M, Feldmeyer D. 2013. Morphology and physiology of excitatory neurons in layer 6b of the somatosensory rat barrel cortex. *Cereb Cortex*. 23:2803–2817.

Marx M, Gunter RH, Hucko W, Radnikow G, Feldmeyer D. 2012. Improved biocytin labeling and neuronal 3D reconstruction. *Nat Protoc*. 7:394–407.

Miller EK, Cohen JD. 2001. An integrative theory of prefrontal cortex function. *Annu Rev Neurosci*. 24:167–202.

Miyoshi G, Young A, Petros T, Karayannis T, McKenzie Chang M, Lavado A, Iwano T, Nakajima M, Taniguchi H, Huang ZJ *et al*. 2015. Prox1 regulates the subtype-specific development of caudal ganglionic eminence-derived GABAergic cortical interneurons. *J Neurosci*. 35:12869–12889.

Mohler H. 2012. The GABA system in anxiety and depression and its therapeutic potential. *Neuropharmacology*. 62:42–53.

Murayama M, Perez-Garci E, Nevian T, Bock T, Senn W, Larkum ME. 2009. Dendritic encoding of sensory stimuli controlled by deep cortical interneurons. *Nature*. 457:1137–1141.

Narayanan RT, Egger R, Johnson AS, Mansvelder HD, Sakmann B, de Kock CP, Oberlaender M. 2015. Beyond columnar organization: cell type- and target layer-specific principles of horizontal axon projection patterns in rat vibrissal cortex. *Cereb Cortex*. 25:4450–4468.

Overstreet-Wadiche L, McBain CJ. 2015. Neurogliaform cells in cortical circuits. *Nat Rev Neurosci*. 16:458–468.

Palmer L, Murayama M, Larkum M. 2012. Inhibitory regulation of dendritic activity in vivo. *Front Neural Circuit*. 6:26.

Palmer LM, Shai AS, Reeve JE, Anderson HL, Paulsen O, Larkum ME. 2014. NMDA spikes enhance action potential generation during sensory input. *Nat Neurosci*. 17:383.

Pandya DN, Yeterian EH. 1990. Prefrontal cortex in relation to other cortical areas in rhesus monkey: architecture and connections. *Prog Brain Res*. 85:63–94.

Perrenoud Q, Rossier J, Geoffroy H, Vitalis T, Gallopin T. 2013. Diversity of GABAergic interneurons in layer VIa and VIb of mouse barrel cortex. *Cereb Cortex*. 23:423–441.

Petrides M, Pandya DN. 1999. Dorsolateral prefrontal cortex: comparative cytoarchitectonic analysis in the human and the macaque brain and corticocortical connection patterns. *Eur J Neurosci*. 11:1011–1036.

Pichon F, Nikonenko I, Kraftsik R, Welker E. 2012. Intracortical connectivity of layer VI pyramidal neurons in the somatosensory cortex of normal and barrelless mice. *Eur J Neurosci*. 35:855–869.

Pronneke A, Scheuer B, Wagener RJ, Mock M, Witte M, Staiger JF. 2015. Characterizing VIP neurons in the barrel cortex of VIPcre/tdTomato mice reveals layer-specific differences. *Cereb Cortex*. 25:4854–4868.

Riga D, Matos MR, Glas A, Smit AB, Spijker S, Van den Oever MC. 2014. Optogenetic dissection of medial prefrontal cortex circuitry. *Front Syst Neurosci*. 8:230.

Rotaru DC, Olezene C, Miyamae T, Povysheva NV, Zaitsev AV, Lewis DA, Gonzalez-Burgos G. 2015. Functional properties of GABA synaptic inputs onto GABA neurons in monkey prefrontal cortex. *J Neurophysiol*. 113:1850–1861.

Rubin AN, Kessaris N. 2013. PROX1: a lineage tracer for cortical interneurons originating in the lateral/caudal ganglionic eminence and preoptic area. *PLoS One*. 8:e77339.

Saha T, Rathmann I, Viplav A, Panzade S, Begemann I, Rasch C, Klingauf J, Matis M, Galic M. 2016. Automated analysis of filopodial length and spatially resolved protein concentration via adaptive shape tracking. *Mol Biol Cell*. 27:3616–3626.

Santana N, Artigas F. 2017. Laminar and cellular distribution of monoamine receptors in rat medial prefrontal cortex. *Front Neuroanat*. 11:87.

Schmitt LI, Wimmer RD, Nakajima M, Happ M, Mofakham S, Halassa MM. 2017. Thalamic amplification of cortical connectivity sustains attentional control. *Nature*. 545:219–223.

Silberberg G, Markram H. 2007. Disynaptic inhibition between neocortical pyramidal cells mediated by Martinotti cells. *Neuron*. 53:735–746.

Stepanyants A, Martinez LM, Ferecsko AS, Kisvarday ZF. 2009. The fractions of short- and long-range connections in the visual cortex. *Proc Natl Acad Sci U S A*. 106: 3555–3560.

Sun Q, Li X, Ren M, Zhao M, Zhong Q, Ren Y, Luo P, Ni H, Zhang X, Zhang C *et al*. 2019. A whole-brain map of long-range inputs to GABAergic interneurons in the mouse medial prefrontal cortex. *Nat Neurosci*. 22:1357–1370.

Tan Z, Hu H, Huang ZJ, Agmon A. 2008. Robust but delayed thalamocortical activation of dendritic-targeting inhibitory interneurons. *Proc Natl Acad Sci U S A*. 105:2187–2192.

Thomson AM. 2010. Neocortical layer 6, a review. *Front Neuroanat*. 4:13.

Thomson AM, Bannister AP, Mercer A, Morris OT. 2002. Target and temporal pattern selection at neocortical synapses. *Philos Trans R Soc Lond Ser B Biol Sci*. 357:1781–1791.

Tremblay R, Lee S, Rudy B. 2016. GABAergic interneurons in the neocortex: from cellular properties to circuits. *Neuron*. 91:260–292.

Uylings HB, Groenewegen HJ, Kolb B. 2003. Do rats have a prefrontal cortex? *Behav Brain Res*. 146:3–17.

Uylings HB, van Eden CG. 1990. Qualitative and quantitative comparison of the prefrontal cortex in rat and in primates, including humans. *Prog Brain Res*. 85:31–62.

van Aerde KI, Feldmeyer D. 2015. Morphological and physiological characterization of pyramidal neuron subtypes in rat medial prefrontal cortex. *Cereb Cortex*. 25:788–805.

van Aerde KI, Mann EO, Canto CB, Heistek TS, Linkenkaer-Hansen K, Mulder AB, van der Roest M, Paulsen O, Brussaard AB, Mansvelder HD. 2009. Flexible spike timing of layer 5 neurons during dynamic beta oscillation shifts in rat prefrontal cortex. *J Physiol*. 587:5177–5196.

Van Eden CG, Uylings HB. 1985. Cytoarchitectonic development of the prefrontal cortex in the rat. *J Comp Neurol*. 241:253–267.

Volk DW, Lewis DA. 2005. GABA targets for the treatment of cognitive dysfunction in schizophrenia. *Curr Neuropharmacol*. 3:45–62.

von Engelhardt J, Khrulev S, Eliava M, Wahlster S, Monyer H. 2011. 5-HT(3A) receptor-bearing white matter interstitial GABAergic interneurons are functionally integrated into cortical and subcortical networks. *J Neurosci*. 31:16844–16854.

Wang Y, Gupta A, Toledo-Rodriguez M, Wu CZ, Markram H. 2002. Anatomical, physiological, molecular and circuit properties of nest basket cells in the developing somatosensory cortex. *Cereb Cortex*. 12:395–410.

Wang Y, Toledo-Rodriguez M, Gupta A, Wu CZ, Silberberg G, Luo JY, Markram H. 2004. Anatomical, physiological and molecular properties of Martinotti cells in the somatosensory cortex of the juvenile rat. *J Physiol-London*. 561:65–90.

Ward JH. 1963. Hierarchical grouping to optimize an objective function. *J Am Stat Assoc*. 58:–236-244.

Weiner DM, Levey AI, Sunahara RK, Niznik HB, O'Dowd BF, Seeman P, Brann MR. 1991. D1 and D2 dopamine receptor mRNA in rat brain. *Proc Natl Acad Sci U S A*. 88:1859–1863.

West DC, Mercer A, Kirchhecker S, Morris OT, Thomson AM. 2006. Layer 6 cortico-thalamic pyramidal cells preferentially innervate interneurons and generate facilitating EPSPs. *Cereb Cortex*. 16:200–211.

Wimmer RD, Schmitt LI, Davidson TJ, Nakajima M, Deisseroth K, Halassa MM. 2015. Thalamic control of sensory selection in divided attention. *Nature*. 526:705–709.

Yavorska I, Wehr M. 2016. Somatostatin-expressing inhibitory interneurons in cortical circuits. *Front Neural Circuit*. 10:76.

Yuste R, Hawrylycz M, Aalling N, Arendt D, Armananzas R, Ascoli G, Bielza C, Bokharaie V, Bergmann T, Bystron I, *et al*. 2019. A community-based transcriptomics classification and nomenclature of neocortical cell types. *arXiv*. 1909.03083.

Zaitsev AV, Povysheva NV, Gonzalez-Burgos G, Rotaru D, Fish KN, Krimer LS, Lewis DA. 2009. Interneuron diversity in layers 2-3 of monkey prefrontal cortex. *Cereb Cortex*. 19:1597–1615.

Zeng H, Sanes JR. 2017. Neuronal cell-type classification: challenges, opportunities and the path forward. *Nat Rev Neurosci*. 18:530–546.

Zhang ZW, Deschenes M. 1997. Intracortical axonal projections of lamina VI cells of the primary somatosensory cortex in the rat: a single-cell labeling study. *J Neurosci*. 17:6365–6379.

Zhang ZW, Deschenes M. 1998. Projections to layer VI of the posteromedial barrel field in the rat: a reappraisal of the role of corticothalamic pathways. *Cereb Cortex*. 8:428–436.

Ziegler DA, Pritchett DL, Hosseini-Varnamkhasti P, Corkin S, Hamalainen M, Moore CI, Jones SR. 2010. Transformations in oscillatory activity and evoked responses in primary somatosensory cortex in middle age: a combined computational neural modeling and MEG study. *NeuroImage*. 52:897–912.

Zikopoulos B, Barbas H. 2006. Prefrontal projections to the thalamic reticular nucleus form a unique circuit for attentional mechanisms. *J Neurosci*. 26:7348–7361.

Zorrilla de San Martin J, Donato C, Peixoto J, Aguirre A, Choudhary V, De Stasi A, Lourenço J, Potier M-C, Bacci A. 2020. Alterations of specific inhibitory circuits of the prefrontal cortex underlie abnormal network activity in a mouse model of down syndrome. *bioRxiv*. 2020.2002.2024. 963041.